This is an *Accepted Manuscript*, which has been through the Royal Society of Chemistry peer review process and has been accepted for publication.

Accepted Manuscripts are published online shortly after acceptance, before technical editing, formatting and proof reading. Using this free service, authors can make their results available to the community, in citable form, before we publish the edited article. We will replace this *Accepted Manuscript* with the edited and formatted *Advance Article* as soon as it is available.

You can find more information about *Accepted Manuscripts* in the **Information for Authors**.

Please note that technical editing may introduce minor changes to the text and/or graphics, which may alter content. The journal's standard **Terms & Conditions** and the **Ethical guidelines** still apply. In no event shall the Royal Society of Chemistry be held responsible for any errors or omissions in this *Accepted Manuscript* or any consequences arising from the use of any information it contains.

Interfacial Interaction of Ag Nanoparticles with Graphene Oxide Supports for Improving NH₃ and NO Adsorption: a First-Principles Study

Shaobin Tang, [*,†]   Weihua Wu, [†]   and Jianping Yu[*,‡]

[†]Key Laboratory of Organo-Pharmaceutical Chemistry of Jiangxi Province, Gannan Normal University, Ganzhou 341000, China
[‡]School of life and environmental sciences, Gannan Normal University, Ganzhou 341000, China

ABSTRACT: We investigated the structural and electronic properties of Ag_{13} nanoparticle (NPs) deposited on graphene oxides (GOs) and the effect of the interfacial interaction on NH_3 and NO adsorption by density functional theory calculations. The epoxy functional group and its neighboring sp^2 carbon atoms of GOs, rather than the hydroxyl group, are used as active sites to enhance the binding of Ag_{13} to graphene through the C–O–Ag and C–Ag chemical bonds. The stability of deposited Ag NPs depends on the chemical environment of active sites in GOs, including the atomic arrangement of epoxides and its concentration. The deposited Ag_{13} NPs are likely to be further oxidized to form $Ag_{13}O$ by neighboring oxygen irrespective of oxidation level of GOs. The strong interfacial interaction of Ag_{13}/GOs, which effectively tunes the position of d-band center of NPs due to large charge transfer from Ag_{13} to GOs, has significant impact on the adsorption of NH_3. The NH_3 is strongly adsorbed on deposited Ag_{13} through the formation of N–Ag bond and NH⋯O hydrogen bond between NH_3 and O from C–O–Ag. The electronic structure calculations show that the hybridization of HOMO orbital of NH_3 with conduction bands of Ag_{13}-GOs results in the strong donor doping by NH_3 molecule, and gives rise to larger charge transfers from NH_3 to hybrid, compared to NH_3 adsorption on isolated Ag_{13} and GOs. The adsorption of NO on oxidized Ag_{13} on GOs is obviously improved due to the oxidation of NO to NO_2 by its neighboring oxygen atoms. In

contrast to NH$_3$, the adsorbed NO acts as acceptor character. The calculated results show good agreement with experimental observations.

_____

* Corresponding author. Fax: +86−797−8393536

E-mail address: tsb1980@xmu.edu.cn, yujianping402871@sina.com

2

1. Introduction

Graphene, a single layer of carbon atoms formed in honeycomb lattice, has attracted considerable interest due to its exceptional electrical,[1,2] thermal,[3] and mechanical[4] properties and potential applications in nanoscale electronics, such as sensors.[5] Because of its high electron mobility, large specific surface area, and low electrical noise at room temperature, graphene is highly sensitive to changes in its chemical environment.[6] Adsorption of external molecular species on graphene, such as NO_2 and NH_3, may change the local carrier concentration and result in remarkable fluctuation of conductivity.[7-9] However, the lack of chemically active defect sites on surface leads to the low sensitivity and poor selectivity of pristine graphene that limits its wide use in practical sensing applications.[5] Functionalized graphene with noble metal nanocrystals (NCs) may represent a new type of hybrid nanostructure, which could display novel physical and chemical properties, improving the performance of sensing devices.[10]

To realizing the high sensing performance, many effective methods have been developed to fabricate graphene-based hybrid structures for gas sensor devices. Owing to the high reaction activity, the noble metal NCs and metal oxides, such as Ag,[11,12] Pd,[13] Au,[14] Pt,[15] and SnO_2,[16,17] are used to decorate the low-dimensional carbon nanomaterials for gas sensing enhancement. Recently, Chen et al. [11] have reported high-performance ammonia sensor using Ag NCs-functionalized multiwalled nanotubes (Ag NC-MWCNTs). It is found that the attached Ag NCs on MWCNTs significantly enhanced sensitivity to NH_3. The density functional theory calculations

(DFT) also revealed that the oxidized Ag surface plays a critical role in the sensor's fast response accompanying a net electron transfer from NH_3 to Ag NC-MWCNTs hybrid.

Recently, many experimental works[18-20] have reported that reduced graphene oxides (rGOs) may provide promising applications for high-performance molecular sensors due to the presence of various active sites and high electrical conductivity. More importantly, the rGOs could be used as an effective support of NCs because the oxygen-containing groups can strongly anchor NCs to the material surface.[16,17, 21-25] It is reported that the GOs can effectively prevent NCs from aggregation, and the Ag NCs deposited on GOs are highly stable. Very recently, Chen et al.[26] fabricated the Ag nanoparticle (NP)-decorated rGOs hybrid nanostructures with higher sensitivity towards NH_3 than that of pristine rGOs and MWCNTs/Ag. Despite these important contributions, experimentally, the detailed mechanisms for sensing performance enhancement using metal-NPs/rGOs still remain unclear.

The properties of the NPs/graphene hybrid strongly depend on its structure. Complete understanding the interface interaction between NCs and graphene is an enormous challenge because NCs can interact with edges and defective sites or functional groups on graphene through covalent and noncovalent bonding. Many previous theoretical studies [27-30] have been devoted to understand the interaction between metal NPs and graphene. Based on DFT calculations, the theoretical works revealed that the presence of dangling bonds at defects leads to strong binding of Pt_{13} [27] and Fe_{13} (or Al_{13})[28] NPs with defective graphene. The interface interfaction of

NPs/graphene modifies the of d-band center position of NPs, which improves the tolerance of Pt cluster to CO poisoning and enhances the catalytic reactivity of Fe_{13} cluster for decomposition of NH_3, respectively. In addition, the strain is applied to graphene support to enhance the interaction with Pt cluster, improving the catalytic properties of nanoclusters.[31] When NPs are supported on rGOs, the NPs/rGOs interface becomes more complex compared with graphene without functional groups because many factors, including atomic structure of oxygen groups and its concentration, determine the interaction of NPs with rGOs.

Relative to NPs/graphene, a little of works on interaction mechanisms for NPs/rGOs are reported. Recently, Ho et al. [32] reveal the important role of oxygen concentration for the stability of Pt_{13} deposited on graphene oxides (GOs). However, the effect of atomic arrangement of epoxy functional group and role of hydroxyl group have never been considered in their works as reported by our previous works.[33] The detailed structural properties of metal NPs-decorated GOs or rGOs nanomaterials are still poorly understood, and an atomic-scale understanding on interfacial interaction of Ag NPs/GOs and its effect on adsorption of gas molecules is highly required for gas sensor devices. In this paper, using DFT calculations, we investigate the binding mechanisms of Ag_{13} NPs supported on GOs, and discuss the effect of interface interaction on NH_3 and NO adsorption.

2. Models and methods

Density functional theory calculations were performed with the DMol3 package [34] **using** the Perdew, Burke, and Ernzerhof (PBE) exchange-correlation functional.[35] The

double numerical plus polarization function (DNP) basis set and a real-space cutoff of 5.0 Å were used. The DFT Semi-core Pseudopots (DSPP) were used for the core treatment of Ag atom. For all systems, the spin-polarized calculations were performed. The rectangular supercells of 3×5 graphene unit cells composed of 60 carbon atoms that obeys the periodic boundary conditions were employed to simulate the GOs surface with different oxidation level. The test calculations show that the more larger supercell sizes give the consistent results for stability of deposited Ag NPs. The Ag_{13} NPs-based systems was separated from its periodic images with a vacuum region of 18 Å in the *z*-direction perpendicular to graphene layer. The integration of Brillouin zone was sampled by 5×5×1 *k*-points within the Monkhorst-Pack scheme.[36] During geometry optimization, all atoms were fully relaxed until the residual forces were less than 10^{-3} au and the total energy was converged to 10^{-5} au.

The structural features of GOs were extensively investigated by both experimental and theoretical works.[37-53] It is commonly accepted that the surface of GOs includes two dominant oxygen species of the hydroxyl (OH) and epoxy (–O–) groups on the basal plane of graphene, while other oxygen species, such as carbonyl and carboxyl groups, are mainly located at edge sites. Based on DFT calculations, many theoretical works[45,51] have revealed that the oxygen-containing groups of GOs are energetically preferable to aggregate together, and the coexistence of hydroxyl and epoxy groups on GOs surface is more likely to occur than the presence of single oxygen group. Moreover, the Fourier transform infrared (FTIR) spectroscopy measurements [22,23] confirms the existences of the abundance of hydroxyl and epoxy groups on the

surface of GOs, which play an important role in the process of nucleation and stabilization of metal NPs on GOs. In our computational models, thus, the atomic structures of GOs or rGOs only contain the hydroxyl and epoxy functional groups on the graphene basal plane.

The structures of GOs with different oxidation concentration are denoted as GO-**m**O (and/or -**n**OH), where **m** and **n** represent the number of epoxide and hydroxyl groups, respectively. The effect of oxygen groups with disordered and ordered phase on Ag NPs deposition on GOs is also discussed. The deposition of Ag_{13} cluster with initial cuboctahedron and icosahedron structures on GOs have comparable stability, whereas the cuboctahedron structures of Ag_{13} show larger structural deformation after deposition compared with the icosahedron one as shown in Figure S1 in Supporting Information. In order to investigate interfacial interaction of Ag NPs with GOs, thus, the Ag_{13} cluster with icosahedral symmetry was only used.[54]

To evaluate the binding strength between Ag_{13} NPs and GOs, the binding energies are calculated by:

$$E_b = [E(NPs) + E(GO)] - E(NPs + GO) \qquad (1)$$

where E(NPs), E(GO), and E(NPs+GO) are total energies of isolated Ag_{13} NPs, GOs, and Ag_{13} NPs-decorated GOs, respectively. For the adsorption of NH_3 and NO on Ag_{13}/GOs, the adsorption energies are calculated by:

$$E_{ad} = E(ads + NPs + GO) - [E(NPs + GO) + E(ads)] \qquad (2)$$

where E(NPs+GO), E(ads), and E(ads+NPs+GO) are total energies of Ag_{13}/GOs

hybrid, free adsorbates NH_3 or NO, and NH_3 or NO-adsorbed Ag_{13}/GOs nanocomposite, respectively. Note that the negative adsorption energies correspond to exothermicity for gas molecule adsorption.

3. Results and discussion

3.1 Geometry and stability of Ag_{13} NPs deposited on GOs

The formation of chemical bonds between GOs and Ag is responsible for high stability of deposited Ag NPs on GOs.[22] Herein, the interaction sites on the GOs basal plane mainly involve the hydroxyl (C–OH) and epoxide (C–O–C) functional groups, although the defective site and other oxygen species may interact with Ag. We first focus on the epoxy groups of GO-mO with m range from 2 to 7, which act as the binding sites for Ag NPs interaction via the C–O–Ag covalent bond or Ag···O coordination bond. When Ag_{13} is supported on GOs, there are various adsorption configurations due to different orientation of NPs relative to GOs (see Figures S1d-f in Supporting Information). The energetically most favorable Ag_{13}/GOs structure with top Ag atom pointing to graphene surface is only considered.

Figures 1a and b and Figures S2a-d show the optimized structures of Ag_{13} supported on GO-mO with m = 2 to 7. Table 1 presents the calculated results. With increasing the number of binding site of epoxide, the binding of Ag_{13} with GOs becomes more stronger because the binding energies of Ag_{13}/GO-mO increase from 1.89 eV for m = 2 to 5.51 eV for m = 6 corresponding to 1 to 4 binding sites, far larger than that of binding Ag_{13} to pristine graphene with only 0.04 eV. The predicted large binding energy for Ag_{13}/GOs hybrid illuminates the highly stable Ag NPs

formed on GOs, which is consistent with the experimental observations.[12,22] However, when the binding sites are further increased to 5 corresponding to GO-7O (Figure S2d), the binding energy is 4.86 eV, smaller than that of GO-6O. This results indicate that an appropriate number of binding sites provided by oxygen groups of GOs are needed to improve the interaction with metal NPs. Our calculations also found that when the number of binding sites is remained, changing the atomic arrangement of active epoxy groups from GO-6O-1 (Figure 1b) to GO-6O-2 (Figure S2c) has less impact on stability of Ag NPs deposited on GOs.

The formation of Ag_{13}/GOs nanocomposite can be understood by the interfacial geometry structures. As shown in Figure 1b and Table 1, the six interfacial Ag atoms near the graphene surface can interact with GOs in the following ways: (a) opening of epoxy ring by its neighboring Ag leads to formation of four C–O–Ag covalent bonds with bond lengths of 2.2-2.3 Å, (b) the Ag⋯O coordination bonds between O of newly-formed C–O–Ag and other neighboring Ag are formed with distance of about 2.49 Å, (c) in particular, the formation of chemical bond between epoxy group and Ag reduce the distance from Ag_{13} to sp^2-carbon network of GOs, leading to covalent C–Ag bond with distance of 2.3 Å. Therefore, three types of chemical bond contribute to the formation of Ag_{13} NPs deposited on GOs surface. This interaction mechanisms are different from previous reports for Pt/GOs,[13,32] in which no Pt⋯O coordination bond and C–Pt bond are formed. After opening of the epoxy ring by Ag atom, some sp^2 carbon atoms of GOs are restored. This results are confirmed by FTIR measurements,[22] in which the aromatic C=C vibrations of GOs increased due to

formation of Ag NPs-GOs nanocomposite. Owing to the interfacial interaction, the morphology of Ag_{13} cluster varies slightly from that of freestanding NPs, while the distance of Ag–Ag bonds close to GOs surface significantly changes (see Figure S3). This distance change may tune activity of Ag atom towards gas molecule adsorption.

We now discuss the effect of hydroxyl group used as the binding site on the stability of Ag_{13} on GOs. For realizing this purpose, we use one and two 1,2-hydroxyl pairs to replace the binding sites of one and two epoxides in GO-6O-1 but remain other active sites, respectively. Figures 1c and d show the optimized structures of Ag_{13} supported on GO-5O-2OH and GO-3O-4OH. Instead of C–O–Ag bonds, the hydrogen bond between Ag and O of C–OH is formed when the hydroxyl group has been the binding site. The binding energies for Ag_{13}/GO-5O-2OH and Ag_{13}/GO-3O-2OH are 4.58 and 3.43 eV (see Table 1), respectively, smaller than that of Ag_{13}/GO-6O-1 with 5.3 eV. This results indicate that the presence of hydroxyl group around Ag_{13} reduces the stability of metal NPs deposited on GOs. When all active sites of epoxides in GO-6O-1 remain unchanged, the adsorbed hydroxyl groups neighboring or away from the epoxides exhibit less influence on the binding strength between Ag_{13} and GOs (see Figure S4). Therefore, to obtain the highly dispersed Ag NPs, it is needed to reduce the ratio of hydroxyl to epoxide groups for the synthesis of GOs substrate.

As discussed above, the epoxide concentration only acting as active adsorption site has been an important factor for improving interaction of Ag NPs with GOs. Herein, we also discuss the effect of epoxy groups located at other carbon site on

stability of deposited Ag_{13}. To investigate the effect, we select Ag_{13}/GO-6O-1 (see

Figure 1b) with high stability as the carbon framework for adsorption of additional

oxygen atoms. The epoxides with different concentrations are randomly attached to

C=C bonds of GO-6O-1, which correspond to GO-**m**O with **m** = 9 to 20. Figure 2 and

Figure S2e-h show the optimized structures of Ag_{13}/GO-**m**O. Table 1 present

summary of calculated results for selected hybrid. The results show that these

epoxides, which are not the binding sites, have also significant effect on the stability

of Ag NPs on GOs, depending not only on the its oxidation level, but also on atomic

arrangement (see table 1). The binding energies of Ag_{13}/GO-**m**O (**m** = 9, 12, and 17)

slightly increase from 5.36 to 5.75 eV, while the binding energies for **m** = 11 and 20

decrease, compared to Ag_{13}/GO-6O-1. In particular, when three different atomic

arrangements of the additional epoxy groups in GO-14O-**i** (**i** = 1 to 3) are considered,

which corresponding to the ratio of oxygen to carbon of 0.47, the Ag_{13}/GO-14O-1

(Figure 2a) and Ag_{13}/GO-14O-2 (Figure 2b) show exceptionally high stability with

binding energies of 6.6 and 7.3 eV, respectively. Such high stability of Ag NPs

deposited on GOs is comparable to the deposition of Fe_{13} NPs on graphene with single

vacancy defect.[28,55]

The atomic configurations of GOs including ordered phase are energetically

more favorable that with disordered models, theoretically,[45] although the preparation

of GOs with such structure is still challenging. Herein, the effect of GOs with ordered

distribution of epoxy groups on Ag NPs deposition is discussed. The structural

models of GOs contain the sp^2 carbon regions separated by sp^3 carbon strips

consisting of 1, 2, and 3 nearest-neighboring armchair epoxy group chains, defined as GO1, GO2, and GO3, respectively. Figure 3 and Figure S5 show the optimized structures for Ag_{13}/GOm. The binding energies of Ag_{13}/GOm (**m** = 1 to 3) are 3.52, 2.72, and 0.96 eV, respectively, much smaller than that of disordered models. This results reveal that the GOs surface with ordered structure of oxygen groups may be unsuitable for Ag NPs deposition.

Recently, the experimental works by Chen et al.[56] revealed that the Ag NPs deposited on MWCNT as high-performance sensor can be facilely oxidized as AgO in air at room temperature. The oxygen atom in AgO improves adsorption of NO_2 on Ag NPs. Herein, we discuss the oxidation of Ag_{13} supported on GO-6O-1 and GO-14O-1 by the neighboring oxygen atom, which correspond to the O/C ratios of 0.2 and 0.47, respectively.

Figure 4 show the geometrical structures for transformation from Ag_{13} to oxidized Ag_{13} ($Ag_{13}O$) on GOs and the relative energies. The deposited Ag_{13} on GOs abstracts the O from neighboring C–O–Ag bond or epoxy group to form $Ag_{13}O$, leading to three almost equivalent Ag–O bonds with distance of about 2.15 Å. The formed $Ag_{13}O$ structures are energetically lower by 0.62 eV for GO-6O-1 and by 1.18 eV for GO-14O-1 than Ag_{13} without oxidation. We used the linear/quadratic synchronous transit (LST/QST) method[57] to estimate the barrier for formation of $Ag_{13}O$ structures as shown in Figure 4. The barrier for the oxidation of Ag_{13} on GO-6O-1 and GO-14O-1 are 0.88 and 0.46 eV, respectively. Such difference can be explained as follows: the structural distortion of $Ag_{13}O$ on GO-6O-1 is more

prominent induced by O migration than that on GO-14O-1 (see Figure 4), and the low

oxygen concentration also contributes to the high barrier. This results indicate that

surface of deposited Ag_{13} is likely to be oxidized by oxygen from GOs substrate at a

wide oxygen concentration, which is consistent with the experimental observations.[12]

Such oxidation of Ag_{13} by GOs is quite distinct from previous reports [32] for Pt_{13}

cluster deposited on GO, in which the neighboring oxygen atoms transfer to Pt_{13}

cluster to form $Pt_{13}O$ only when the ratio of oxygen to carbon in GOs is smaller than

0.125.

3.2 Electronic properties of Ag_{13}/GOs hybrids

To understand the details of the interaction between the Ag_{13} and GOs, the

spin-polarized total density of states (TDOS) and projected DOS (PDOS) of selected

Ag, O, and C atoms (labeled in Figures 2a and 1b) of Ag_{13}/GO-6O-1 before and after

interaction have been analyzed as shown in Figure 5. Comparing with isolated Ag_{13}

NPs, the adsorbed Ag_{13} show broader and strongly modified d band ranging from -5

to -3.2 eV with respect to the Fermi level (Figures 5a1 and 5a2). This strong broad

peaks of d states are mainly contributed by the Ag atoms of 4 and 5 layers of Ag_{13}

connecting with O and C atoms, rather than other Ag atoms away from the GOs (see

Figure 5a4).

On the other hand, the strong interaction of Ag_{13} NPs with GOs is reflected by

changes of PDOS of O and C atoms near NPs. Two strong peaks of p states of O1

atom are shift to higher energy level after Ag interaction (Figures 5b1 and b2). In

particular, the p states of O2 atom only remain one strong peak located at 0.7 eV

below the Fermi level and the other peak disappears (Figure 5b3). Such difference indicates that the interaction mechanisms between Ag and O1, and O2 atoms distinctly differ from each other: the former is due to formation of both C–O–Ag and Ag⋯O bonds, the latter is only single C–O–Ag bond. At last, the peaks of p states of carbon connecting with Ag in energy range of -5 to -3 eV relative to the Fermi level become more wider and stronger (Figure 5b5) compared with this carbon without such Ag interaction (Figure 5b4). This results indicate a strong hybridization of the Ag$_{13}$ NPs with the p orbitals of epoxide and sp^2-hybridized carbon atoms. The TDOS caluclations (Figure S6) show that the semiconducting GOs with lower oxidation level become metallic after Ag$_{13}$ interaction, while the semiconducting properties of GOs with high oxidation level are unchanged.

To understand strong binding of Ag$_{13}$ to GOs, the charge density difference for Ag$_{13}$/GOs-6O-1 and Ag$_{13}$/GOs-14O-1, $\Delta\rho = \rho(Ag_{13} - GO) - \rho(Ag_{13}) - \rho(GO)$, is calculated as shown Figures 6a and b, where $\rho(Ag_{13} - GO)$, $\rho(Ag_{13})$, and $\rho(GO)$ represent the total charge densities of Ag$_{13}$-decorated GOs, isolated Ag$_{13}$, and GOs, respectively. From Figures 6a and b, the adsorption of Ag$_{13}$ on GOs induce redistribution of the charge densities. Strong electron accumulation is observed at the neighboring oxygen and carbon atoms near the Ag$_{13}$, whereas the electron depletion is appeared mainly on six Ag atoms attached to GOs surface. This indicates that the deposited Ag$_{13}$ NPs donate electrons to neighboring oxygen and carbon atoms. Owing to electron transfer from Ag to GOs, the magnetic moments of Ag$_{13}$ are reduced from 5.0 μ_B for the isolated structure to 0.26 μ_B for Ag$_{13}$/GOs-6O-1 and 0.46 μ_B for

Ag$_{13}$/GOs-14O-1. Previous results [28,55,58] also reported that the spin polarized

electrons of isolated Fe$_{13}$ NPs or Fe atoms are transferred to graphene surface after

metal adsorption, leading to magnetic moment reduction of metal.

To quantitatively compare transferred electrons between the Ag$_{13}$ NPs and GOs,

the Mulliken population analyses are carried out. As shown in Table 1, the large

charge transfers (-1.61 ~ -1.96 e) from Ag$_{13}$ to GOs are occurred, suggesting strong

interaction between NPs and GOs. These transferred electrons from Ag$_{13}$ can lead to

hole depletion of GOs, which is consistent with the increased resistance of GOs as its

surface is decorated by Ag NPs reported by the experimental observations.[12] Table 2

summarizes the excess charges of Ag$_{13}$-GOs hybrid over isolated NPs and GOs for

atoms labeled in Figure 2b and 1a. It notes that the average excess charges for the five

Ag atoms in 2 and 4 layers of NPs shown in Figure 2b are calculated. Charge analyses

reveal that the Ag4 and Ag5 atoms have the large negative excess charges of about

-0.26 e, while O1 and O2 atoms show large positive excess charges of 0.2–0.25 e, and

C1 atom also shows a significant excess charges of 0.08 e. This indicates that the

electrons are transferred from the bound Ag atoms to its neighboring O and C atoms,

leading to formation of C–O–Ag and C–Ag bonds.

The electronic properties of Ag$_{13}$ clusters are also well tuned by interfacial

interaction with GOs. The d-band centre (ε_d) provides a good measure of chemical

reactivity of transition metal surface.[59] Table 2 also shows the ε_d of Ag atoms for Ag$_{13}$

supported on GOs-6O-1 and GOs-14O-1. All of the Ag atoms in the isolated Ag$_{13}$

show the same ε_d of -3.9 eV, except for the centered Ag atom due to the structure

symmetry. When the Ag_{13} is adsorbed on GOs, the centered Ag3 atom has the lowest ε_d (-5.22 eV for GOs-6O-1 and -4.58 eV GOs-14O-1) among all Ag atoms, followed by Ag1 and Ag2. Therefore, the interface interaction of GOs/NPs well modifies the position of ε_d of Ag_{13}. Such changes in ε_d of adsorbed Ag NPs can be understood by the excess charges of Ag atom after interaction with GOs. As shown in Table 2, the ε_d of Ag increase with increasing the its negative excess charges.

3.3 Adsorption of NH_3 on Ag_{13} NPs supported on GOs

To understand the sensing mechanism of Ag NPs-GOs hybrid as high-performance sensor for gas molecule detection, we investigate the interactions of ammonia with Ag_{13}/GOs nanocomposite. The Ag_{13}/GO-6O-1 with low oxidation level (Figure 1b) and the Ag_{13}/GO-14O-1 with high oxidation level (Figure 2a) are used to simulate the nanocomposite for NH_3 adsorption. The Ag NPs may be the dominant active adsorption sites in Ag_{13}/GOs hybrid sensor. Because the modified electronic properties of Ag NPs are site-dependent, we consider three type of sites Ag1, Ag2, and Ag4 for NH_3 adsorption, where the Ag atoms belong to the 1, 2, and 4 layers of Ag_{13} as labeled in Figure 2b, respectively. The initial configuration of NH_3 with N pointing to Ag atom is considered because other configurations are less stable in energy.

Figures 7 and Table 3 display the optimized structures and calculated results for NH_3 adsorption. For isolated Ag_{13}, the adsorption energy of NH_3 is -0.41 eV. When the binding site for NH_3 adsorption on Ag_{13}/GO-14O-1 only involves the Ag atom, the NH_3 molecules are preferentially adsorbed at Ag4 atom (Figure 7c) because the

adsorption energy is estimated to be -0.86 eV, larger than NH_3 adsorption on Ag1

(Figure 7a) and Ag2a (Figure 7b) sites with corresponding adsorption energies of

-0.66 and -0.8 eV. The most energetically favorable adsorption site of Ag4 is

correlated with its d-band centre more closer to the Fermi level than other Ag1 and

Ag2 atoms (table 2). Such adsorption of NH_3 on Ag NPs leads to formation N–Ag

bond with distance of 2.31-2.39 Å.

Interestingly, when NH_3 is adsorbed on another Ag2b site with the same 2 layer as

Ag2a site (Figure 7d), the adsorption energy is increased to -0.99 eV from -0.8 eV for

Ag2a site, larger than that of NH_3 on pristine GOs and Ag NPs-MWCNTs with

adsorption energies of -0.87 [60] by the LDA functional and -0.36 eV by the PBE

functional,[11] respectively. From Figure 7d, besides the N–Ag bond, the improved

adsorption is also attributed to the formation of hydrogen bond between H of

adsorbed NH_3 and O of single C—O2—Ag bond with distance of 1.94 Å. Such

interaction mechanisms are different from the adsorption of NH_3 on MWCHTs/Ag

hybrid, in which the NH_3 is attracted to hollow sites on oxidized Ag surface with H

pointing to Ag atoms.

In addition, we also calculated adsorption of NH_3 on selected pristine GOs models

using the same PBE functional as shown in Table S1 and Figures 7Sa and b. Owing to

the formation of hydrogen bond OH···N between the hydroxyl group and NH_3, the

highest adsorption energy of NH_3 on pristine GOs is -0.56 eV, and the corresponding

charge transfer from NH_3 to substrate is 0.09 e, smaller than these adsorptions on

Ag_{13}/GOs. This results suggest that the interfacial interaction between NH_3 and GOs

is enhanced by the deposition of Ag NPs.

The adsorption and dissociation of NH_3 on oxidized Ag_{13} are energetically less favorable than on Ag_{13} without oxidation at the same site (Figures 7g-h and table 3). However, these adsorptions of NH_3 on $Ag_{13}O$ are still stronger than that on pristine GOs because the adsorption energy for the former (-0.67 eV) is larger than the latter (see Table S1). For comparison, we also performed the calculations on adsorption of NH_3 on $Ag_{13}O/GO-13O$ using the LDA functional.[61] The results show that the adsorption of NH_3 on pristine GOs (adsorption energy of -0.87 eV)[60] is also improved due to the interfacial interaction between $Ag_{13}O$ and GOs (-1.2 eV) by the LDA functional. Therefore, compared with isolated Ag_{13} and GOs, the Ag_{13}/GOs hybrid shows more stronger adsorption ability for NH_3, which is responsible for the significant sensing enhancement reported by experimental works.[12] The NH_3 adsorptions on $Ag_{13}/GO-6O-1$ with low oxygen concentration are similar with that of GO-14O-1 (see Figures 7e-f and table 3).

To further investigate the possibility of adsorption of NH_3 on Ag NPs/GOs, we estimate the diffusion barriers of the adsorbed NH_3 on deposited Ag_{13}. The diffusion paths of adsorbed NH_3 at various Ag sites: **1→2a** (Figure 7a) and **2a→2b** (Figure 7b), are selected. Calculations indicate that the diffusion barriers for these two pathways are 10.8–11.3 kcal/mol, comparable with 9.2 kcal/mol for NH_3 on isolated Ag_{13} cluster. This results suggest that NH_3 molecules can diffuse on deposited Ag NPs on GOs easily and rapidly.

Previous theoretical works show that adsorption of NH_3 on pristine graphene[62]

and CNTs [63] leads to little charge transfer between them. Our charge population analyses (Table 4) show that comparing with isolated Ag_{13}, the larger charge transfers of 0.23-0.25 e from NH_3 to Ag_{13}/GOs are obtained due to the interfacial interaction, suggesting that the adsorbed NH_3 acts as an electron donor. The charge density difference (Figure 6c) further confirms the electron transfers mainly from NH_3 to Ag NPs. The charge densities of NH_3 adsorbed system are redistributed with the electron accumulation mainly occurred on Ag_{13} and electron depletion on NH_3. Based on the charge population, the electrons of Ag_{13} donated by NH_3 can partially transfer to GO-14O-1 (about 0.06 e), resulting in depletion of holes in GOs. The NH_3-induced donor doping in Ag_{13}-GOs hybrid may lead to the remarkable fluctuation of conductivity, enhancing the sensor response as shown experimentally.[12]

To have an insight into the sensor mechanism for Ag NPs-GOs hybrid for NH_3 detection, we calculated the the spin-polarized TDOS and PDOS of NH_3 and Ag_{13}/GO-14O-1 before and after NH_3 adsorption as shown in Figure 8a. The NH_3 adsorption on Ag_{13}-GOs hybrid increase the spin-polarized DOS at the Fermi level for both spin up and spin down in comparison to that of this hybrid without NH_3 adsorption. The upshift of the Fermi level of NH_3-adsorbed system relative to Ag NPs-GO hybrid suggests the donor doping of adsorbed NH_3. From the DOS of NH_3 before adsorption, the HOMO orbital of free NH_3 is located at 0.5 eV below the Fermi level, and no unoccupied states close to the Fermi level appear. When NH_3 interacts with Ag NPs deposited on GOs, the hybridization of HOMO of NH_3 for both spin channels with conduction bands of Ag_{13}-GOs results in unoccupied states close to the

Fermi level, suggesting electron transfers of 0.21 e from NH_3 to Ag_{13}-GOs. Meanwhile, the HOMO orbital of NH_3 shifts downward to about -2 eV below the Fermi level after adsorption.

3.4 Adsorption of NO on Ag_{13} NPs supported on GOs

We now investigate interaction of another gas molecule, e.g. NO, with Ag_{13}-GOs hybrid. The same adsorption sites and structural models with NH_3 adsorption are considered for NO adsorption. Figures 9 and Table 4 display the optimized structures for selected systems and the calculated results. Compared with isolated Ag_{13}, the adsorption of NO on Ag_{13}-GOs hybrid is less improved by the interfacial interaction with the highest adsorption energies of only -0.55 eV for Ag_{13}/GO-14O-1 (Figure 9a) and -0.64 eV for Ag_{13}/GO-6O-1 (Figure 9c), but still stronger than that on pristine GOs (see Table S1 and Figure S7c and d). The corresponding charge transfers from NO to Ag_{13}-GOs are -0.08 and -0.09 e, smaller than that to isolated Ag_{13} (see Table 4). The DOS calculations (Figure 8b) for NO-adsorbed systems show that the adsorption of NO has less impact on the DOS of Ag_{13}-GOs hybrid near the Fermi level. This results indicate that the sensing performance of Ag NPs/GOs may be lower than the isolated NPs for NO detection. In contrast to NH_3 adsorption, the charge density difference (see Figure 6d) and the DOS and PDOS calculations of NO before and after adsorption (Figure 8b) confirm the acceptor character of adsorbed NO on Ag NPs-GOs.

Interestingly, when Ag NPs deposited on GOs are oxidized as $Ag_{13}O$ as discussed above, the adsorption of NO on $Ag_{13}O$ can be largely improved due to the oxidation

of NO to NO$_2$. As shown in Figures 9b and d, the O attached to Ag$_{13}$ transfers to its neighboring N of adsorbed NO to form NO$_2$-like species, leading to oxidation of NO. The oxidation of NO on Ag$_{13}$O/GOs hybrid is more favorable in energy by 1.13 eV for GO-14O-1 (Figure 9b) and 1.31 eV for GO-6O-1 (Figure 9d) than that NO adsorption on Ag$_{13}$O. The reaction pathways indicate that the oxidation of NO to NO$_2$ can occur with a moderate energy barrier of 0.68 eV (see Figure S8). The corresponding charge transfers from NO to Ag$_{13}$O/GOs hybrid are increased to -0.15 and -0.16 e, which are larger than that to isolated Ag$_{13}$ and GOs, suggesting stronger acceptor doping of adsorbed NO. The increased interaction of NO with Ag$_{13}$O/GOs is also supported by the DOS calculations (Figure S9) due to the formation of NO$_2$. Thus, the Ag$_{13}$O/GOs hybrids may present the high sensing-performance for NO detection.

4. Conclusions

We investigated the stability of Ag$_{13}$ NPs deposited on GOs and the effect of their interfacial interaction on NH$_3$ and NO adsorption by the first-principles calculations. The Ag$_{13}$ NPs can be strongly bound to the GOs surface with binding energies up to 7.3 eV. The presence of epoxy groups of GOs, rather than the hydroxyl group, play an important role for improving the stability of Ag$_{13}$ NPs deposited on GOs, depending on its chemical environment. The hybridization of d states of Ag$_{13}$ with p states of its neighboring epoxides and sp^2 carbon atoms lead to the formation of C–O–Ag and C–Ag bonds accompanying large charge transfers from Ag NPs to GOs. The deposited Ag$_{13}$ NPs are **energetically preferable** to be further oxidized to form

Ag$_{13}$O by its neighboring O atom **irrespective of** oxidation level of GOs.

The strong interfacial interaction of Ag$_{13}$/GOs obviously improves the adsorption of NH$_3$ on Ag$_{13}$ NPs, leading to formation of N–Ag bond and hydrogen bond NH$\cdots$O between NH$_3$ and O from C–O–Ag. The PDOS calculations reveal that the strong hybridization of HOMO orbital of NH$_3$ with conduction bands of Ag$_{13}$-GOs results in deep donor doping to this hybrid. The enhanced adsorption of NH$_3$ and improved charge transfers from NH$_3$ to Ag$_{13}$-GOs may be responsible for the high sensitivity and fast response for Ag NPs-GOs hybrid sensor towards NH$_3$ as observed experimentally. The adsorption of NO on oxidized Ag$_{13}$ is obviously improved due to the oxidation of NO to NO$_2$ by its neighboring oxygen atoms. Present results provide the fundamental understanding for sensing mechanisms of metal NPs-GOs hybrid as chemical sensor.

Electronic Supplementary Information (ESI) available: Optimized structures and corresponding binding energies for other Ag$_{13}$/GOs hybrids, DOS of several GOs-related systems, and (P)DOS for oxidation of NO on Ag$_{13}$O/GOs. See DOI:

Physical Chemistry Chemical Physics Accepted Manuscript

10.1039/b000000x/

References

1 K. S. Novoselov, A. K. Geim, S. V. Morozov, D. Jiang, Y. Zhang, S. V. Dubonos, I. V. Grigorieva and A. A. Firsov, *Science,* 2004, **306**, 666-669.

2 Y. B. Zhang, Y. W. Tan, H. L. Stormer and P. Kim, *Nature,* 2005, **438**, 201-204.

3 A. A. Balandin, S. Ghosh, W. Z. Bao, I. Calizo, D. Teweldebrhan, F. Miao and C. N. Lau, *Nano Lett.,* 2008, **8**, 902-907.

4 I. W. Frank, D. M. Tanenbaum, A. M. Van der Zande and P. L. McEuen, *J. Vac. Sci. Technol. B,* 2007, **25**, 2558-2561.

5 F. Schedin, A. K. Geim, S. V. Morozov, E. W. Hill, P. Blake, M. I. Katsnelson and K. S. Novoselov, *Nat. Mater.,* 2007, **6**, 652-655.

6 F. Yavari and N. Koratkar, *J. Phys. Chem. Lett.,* 2012, **3**, 1746-1753.

7 P. Qi, O. Vermesh, M. Grecu, A. Javey, Q. Wang, H. Dai, S. Peng and K. J. Cho, *Nano Lett.,* 2003, **3**, 347-351.

8 T. O. Wehling, K. S. Novoselov, S. V. Morozov, E. E. Vdovin, M. I. Katsnelson, A. K. Geim and A. I. Lichtenstein, *Nano Lett.,* 2008, **8**, 173-177.

9 A. Sakhaee-Pour, M. T. Ahmadian and A. Vafai, *Solid State Commun.,* 2008, **147**, 336-340.

10 S. Cui, S. Mao, G. Lu and J. Chen, *J. Phys. Chem. Lett.,* 2013, **4**, 2441-2454.

11 S. M. Cui, H. H. Pu, G. H. Lu, Z. H. Wen, E. C. Mattson, C. Hirschmugl, M.

Gajdardziska-Josifovska, M. Weinert and J. H. Chen, *ACS Appl. Mater. Interfaces,*

2012, **4**, 4898-4904.

12 S. M. Cui, S. Mao, Z. H. Wen, J. B. Chang, Y. Zhang and J. H. Chen, *Analyst,*

2013, **138**, 2877-2882.

13 W. Li, X. Geng, Y. Guo, J. Rong, Y. Gong, L. Wu, X. Zhang, P. Li, J. Xu, G.

Cheng, M. Sun and L. Liu, *ACS Nano,* 2011, **5**, 6955-6961.

14 J. B. Chang, S. Mao, Y. Zhang, S. M. Cui, D. A. Steeber and J. H. Chen, *Biosens.*

Bioelectron., 2013, **42**, 186-192.

15 B. H. Chu, C. F. Lo, J. Nicolosi, C. Y. Chang, V. Chen, W. Strupinski, S. J.

Pearton and F. Ren, *Sens. Actuators B,* 2011, **157**, 500-503.

16 S. Mao, S. M. Cui, G. H. Lu, K. H. Yu, Z. H. Wen and J. H. Chen, *J. Mater.*

Chem., 2012, **22**, 11009-11013.

17 P. A. Russo, N. Donato, S. G. Leonardi, S. Baek, D. E. Conte, G. Neri and N.

Pinna, *Angew. Chem., Int. Ed.,* 2012, **51**, 11053-11057.

18 J. D. Fowler, M. J. Allen, V. C. Tung, Y. Yang, R. B. Kaner and B. H. Weiller,

ACS Nano, 2009, **3**, 301-306.

19 Y. Dan, Y. Lu, N. J. Kybert, Z. Luo and A. T. C. Johnson, *Nano Lett.,* 2009, **9**,

1472-1475.

20 J. T. Robinson, F. K. Perkins, E. S. Snow, Z. Wei and P. E. Sheehan, *Nano Lett.,*

2008, **8**, 3137-3140.

21 G. Zhou, J. Chang, S. Cui, H. Pu, Z. Wen and J. Chen, *ACS Appl. Mater.*

Interfaces, 2014, **6**, 19235–19241.

22 W. Shao, X. Liu, H. Min, G. Dong, Q. Feng and S. Zuo, *ACS Appl. Mater.*

Interfaces, 2015, **7**, 6966-6973.

23 Y.-X. Huang, J.-F. Xie, X. Zhang, L. Xiong and H.-Q. Yu, *ACS Appl. Mater.*

Interfaces, 2014, **6**, 15795-15801.

24 S. K. Bhunia and N. R. Jana, *ACS Appl. Mater. Interfaces,* 2014, **6**, 20085-20092.

25 Y. Chen, Q.-L. Zhu, N. Tsumori and Q. Xu, *J. Am. Chem. Soc.,* 2015, **137**,

106-109.

26 S. M. Cui, S. Mao, Z. H. Wen, J. B. Chang, Y. Zhang and J. H. Chen, *Analyst,*

2013, **138**, 2877-2882.

27 I. Fampiou and A. Ramasubramaniam, *J. Phys. Chem. C,* 2013, **117**,

19927–19933.

28 D.-H. Lim, A. S. Negreira and J. Wilcox, *J. Phys. Chem. C,* 2011, **115**,

8961–8970.

29 H. Vedala, D. C. Sorescu, G. P. Kotchey and A. Star, *Nano Lett.,* 2011, **11**,

2342-2347.

30 W. Gao, J. E. Mueller, J. Anton, Q. Jiang and T. Jacob, *Angew. Chem. Int. Ed.,*

2013, **52**, 1-6.

31 G. Kim, Y. Kawazoe and K.-R. Lee, *J. Phys. Chem. Lett.,* 2012, **3**, 1989-1996.

32 S.-Y. Wu and J.-J. Ho, *J. Phys. Chem. C,* 2014, **118**, 26764–26771.

33 S. Tang and J. Zhu, *RSC Adv.,* 2014, **4**, 23084–23096.

34 B. Delley, *J. Chem. Phys.,* 1990, **92**, 508.

35 J. P. Perdew, K. Burke and M. Ernzerhof, *Phys. Rev. Lett.,* 1996, **77**, 3865.

36 H. J. Monkhorst and J. D. Pack, *Phys. Rev. B,* 1976, **13**, 5188.

37 S. Watcharotone, D. A. Dikin, S. Stankovich, R. Piner, I. Jung, G. H. B. Dommett, G. Evmenenko, S.-E. Wu, S.-F. Chen, C.-P. Liu, S. T. Nguyen and R. S. Ruoff, *Nano Lett.,* 2007, **7**, 1888-1892.

38 G. Eda, G. Fanchini and M. Chhowalla, *Nat. Nanotechnol.,* 2008, **3**, 270-274.

39 H. A. Becerril, J. L. Mao, Z., R. M. Stoltenberg, Z. Bao and Y. Chen, *ACS Nano,* 2008, **2**, 463-470.

40 G. Eda, Y.-Y. Lin, S. Miller, C.-W. Chen, W.-F. Su and M. Chhowalla, *Appl. Phys. Lett.,* 2008, **92**, 233305.

41 J. Wu, H. A. Becerril, Z. Bao, Z. Liu, Y. Chen and P. Peumans, *Appl. Phys. Lett.,* 2008, **92**, 263302.

42 W. Cai, R. D. Piner, F. J. Stadermann, S. Park, M. A. Shaibat, Y. Ishii, D. Yang, A. Velamakanni, S. J. An, M. Stoller, J. An, D. Chen and R. S. Ruoff, *Science,* 2008, **321**, 1815-1817.

43 A. Bagri, R. Grantab, N. V. Medhekar and V. B. Shenoy, *J. Phys. Chem. C,* 2010, **114**, 12053-12061.

44 A. Bagri, C. Mattevi, M. Acik, Y. J. Chabal, M. Chhowalla and V. B. Shenoy, *Nat. Chem.,* 2010, **2**, 581-587.

45 J.-A. Yan, L. Xian and M. Y. Chou, *Phys. Rev. Lett.,* 2009, **103**, 086802.

46 W. Zhang, V. Carravetta, Z. Li, Y. Luo and J. Yang, *J. Chem. Phys.,* 2009, **131**, 244505.

47 Z. Li, W. Zhang, Y. Luo, J. Yang and J. G. Hou, *J. Am. Chem. Soc.,* 2009, **131**,

6320-6321.

48 A. Lerf, H. He, M. Forster and J. Klinowski, *J. Phys. Chem. B,* 1998, **102**,

4477-4482.

49 X. Li, G. Zhang, X. Bai, X. Sun, X. Wang, E. Wang and H. Dai, *Nat. Nanotechnol.,*

2008, **3**, 538-542.

50 W. Gao, L. B. Alemany, L. Ci and P. M. Ajayan, *Nat. Chem.,* 2009, **1**, 403-408.

51 J.-A. Yan and M. Y. Chou, *Phys. Rev. B,* 2010, **82**, 125403.

52 H.-K. Jeong, Y. P. Lee, R. J. W. E. Lahaye, M.-H. Park, K. H. An, I. J. Kim, C.-W.

Yang, C. Y. Park, R. S. Ruoff and Y. H. Lee, *J. Am. Chem. Soc.,* 2008, **130**,

1362-1366.

53 K.-Y. Lian, Y.-F. Ji, X.-F. Li, M.-X. Jin, D.-J. Ding and Y. Luo, *J. Phys. Chem. C,*

2013, **117**, 6049-6054.

54 Y. Rao, Y. Lei, X. Cui, Z. Liu and F. Chen, *Journal of Alloys and Compounds,*

2013, **565**, 50-55.

55 X. Liu, C. Meng and Y. Han, *Phys. Chem. Chem. Phys.,* 2012, **14**, 15036-15045.

56 S. Cui, H. Pu, E. C. Mattson, G. Lu, S. Mao, M. Weinert, C. J. Hirschmugl, M.

Gajdardziska-Josifovskab and J. Chen, *Nanoscale,* 2012, **4**, 5887–5894.

57 N. Govind, M. Petersen, G. Fitzgerald, D. king-Smith and Andzelm, *J.*

Comput. Mater. Sci., 2003, **28**, 250.

58 K. T. Chan, J. B. Neaton and M. L. Cohen, *Phys. Rev. B,* 2008, **77**, 235430.

59 B. Hammer and J. K. Nørskov, *Surf. Sci.,* 1995, **343**, 211-220.

60 S. Tang and Z. Cao, *J. Phys. Chem. C,* 2012, **116**, 8778-8791.

28

61 J. P. Perdew and Y. Wang, *Phys. Rev. B*, 1992, **45**, 13244.

62 O. Leenaerts, B. Partoens and F. M. Peeters, *Phys. Rev. B,* 2008, **77**, 125416.

63 H. Chang, J. D. Lee, S. M. Lee and Y. H. Lee, *Appl. Phys. Lett.,* 2001, **79**, 3863.

Table 1: Summary of calculated results for the Ag$_{13}$ deposited on GOs substrate with different oxygen concentration: the binding energy (E_b), the minimum (d_{min}) and maximum (d_{max}) distance from O to Ag, the distance of Ag–C bond, and the charge transfers from Ag$_{13}$ to GOs.

substrate	E_b (eV)	d_{min}/d_{max} (Å)	d_{Ag-C} (Å)	ΔQ (e)
GO-2O	1.89	2.3/2.43	2.52	0.82
GO-3O	3.23	2.26/2.51	2.64	1.06
GO-5O	4.2	2.26/2.46	2.33	1.41
GO-6O-1	5.3	2.2/2.49	2.3	1.61
GO-6O-2	5.51	2.28/2.43	2.46	1.7
GO-5O-2OH	4.58	2.48/2/26	2.31	1.45
GO-3O-4OH	3.43	2.2/2.69	2.38	1.16
GO-5O-2OH-2	5.19	2.26/2.56	2.34	1.64
GO-9O	5.36	2.18/2.44	2.34	1.74
GO-11O	4.38	2.17/2.46	2.35	1.71
GO-12O	5.42	2.16/2.5	2.36	1.86
GO-14O-1	6.6	2.17/2.59	2.36	1.89
GO-14O-2	7.31	2.16/2.46	2.37	1.89
GO-14O-3	5.52	2.16/2.48	2.34	1.88
GO-17O	5.75	2.16/2.45	2.34	1.96
GO-20O	4.65	2.18/2.47	2.35	2.03

Table 2: The d-band center ε_d (in eV) of Ag and excess charge ΔQ (in e) over the isolated Ag$_{13}$ cluster and GOs for atoms labeled in Figures 1b and 2a.

substrate	property	Ag1	Ag2	Ag3	Ag4	Ag5	Ag/Ag$_{13}$	O1	O2	C1
GO-6O-1	ε_d	-4.06	-4.23	-5.22	-3.71	-3.94	-3.9*			
	ΔQ	-0.03	-0.05	0.06	-0.24	-0.25		0.23	0.21	0.09
GO-14O-1	ε_d	-3.89	-4.04	-4.58	-3.55	-3.58				
	ΔQ	-0.03	-0.07	0.08	-0.27	-0.27		0.25	0.2	0.07

* All atoms of isolated Ag$_{13}$ cluster have the same ε_d except for the centred Ag due to the symmetry of structure.

Table 3: Summary of calculated results for adsorption of NH$_3$ on Ag$_{13}$ deposited on GOs at different sites labeled in Figure 2a: the adsorption energy (E_{ad} in eV), the distance (d in Å) between Gas molecule and Ag, and the charge transfers from the molecule to Ag$_{13}$-GOs hybrid (ΔQ in e).

structure	site	E_{ad}	d	ΔQ (e)
Ag$_{13}$	*	-0.41	2.34	0.18
Ag$_{13}$/GO-14O-1	1	-0.66	2.39	0.18
Ag$_{13}$/GO-14O-1	2a	-0.8	2.32	0.21
Ag$_{13}$/GO-14O-1	4	-0.86	2.31	0.23
Ag$_{13}$/GO-14O-1	2b	-0.99	2.27	0.25
Ag$_{13}$O/GO-13O	2a	-0.67	2.35	0.18
Ag$_{13}$/GO-6O-1	1	-0.65	2.4	0.18
Ag$_{13}$/GO-6O-1	2a	-0.74	2.33	0.2
Ag$_{13}$/GO-6O-1	2b	-0.96	2.31	0.21
Ag$_{13}$O/GO-5O	2a	-0.63	2.35	0.17

* All Ag atoms of isolated Ag$_{13}$ are equivalent to each other except for the centred Ag.

Table 4: Summary of calculated results for adsorption of NO on Ag$_{13}$ deposited on GOs at different sites: the adsorption energy (E_{ad} in eV), the distance (d in Å) between Gas molecule and Ag, and the charge transfers from the molecule to Ag$_{13}$-GOs hybrid (ΔQ in e).

substrate	site	E_{ad}	d	ΔQ (e)
Ag$_{13}$	*	-0.54	2.15	-0.11
Ag$_{13}$/GO-14O-1	1	-0.33	2.26	-0.04
Ag$_{13}$/GO-14O-1	2	-0.55	2.18	-0.08
Ag$_{13}$/GO-14O-1	4	-0.44	2.22	-0.02
Ag$_{13}$O/GO-13O-a	2	-0.43	2.18	-0.02
Ag$_{13}$O/GO-13O-b	2	-1.56	2.29	-0.15
Ag$_{13}$/GO-6O-1	1	-0.36	2.25	-0.06
Ag$_{13}$/GO-6O-1	2	-0.64	2.16	-0.09
Ag$_{13}$O/GO-5O-a	2	-0.5	2.14	-0.08
Ag$_{13}$O/GO-5O-b	2	-1.87	2.28	-0.16

* All Ag atoms of isolated Ag$_{13}$ are equivalent to each other except for the centred Ag.
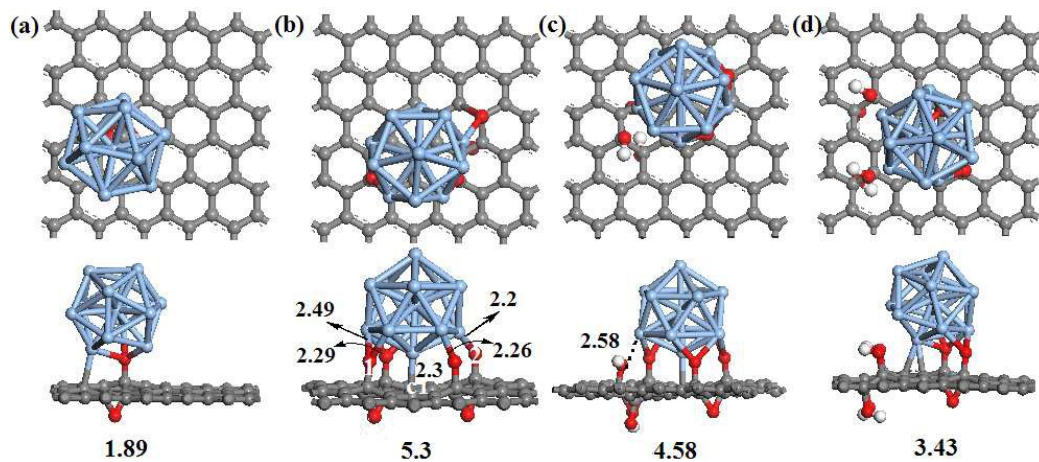
Figure 1 Top and side views of optimized structures (distance in Å) and corresponding binding energies (in eV) for Ag_{13}/GOs hybrid with low oxidation level. (a) Ag_{13}/GO-2O, (b) Ag_{13}/GO-6O-1, (c) Ag_{13}/GO-5O-2OH, and (d) Ag_{13}/GO-3O-4OH. The number in (b) denotes the site of oxygen and carbon atoms.
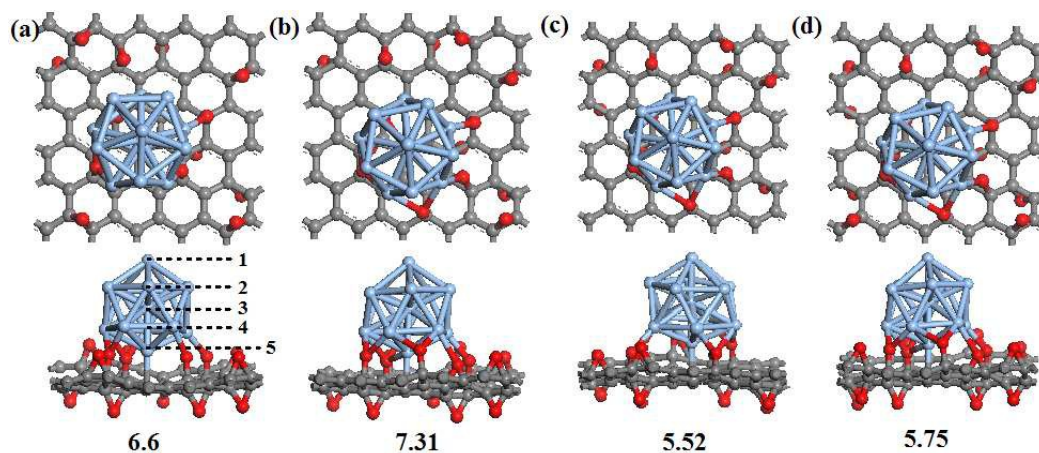
Figure 2 Top and side views of optimized structures and corresponding binding energies (in eV) for Ag_{13}/GOs hybrid with high oxidation level. (a)-(c) Ag_{13}/GO-14O-**i**, where **i** = 1, 2, and 3, represent three different atomic arrangements of other 8 oxygen atoms except for the binding sites, respectively, and (d) Ag_{13}/GO-17O. The number in (a) denotes the different Ag layer of deposited Ag_{13} relative to GOs surface.
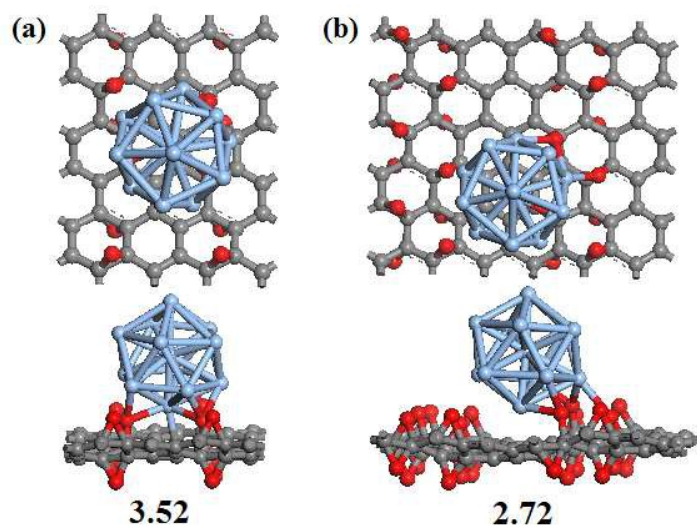
Figure 3 Top and side views of optimized structures and corresponding binding energies (in eV) for Ag_{13} deposited on GOs with ordered phase of epoxides: one armchair sp^2 carbon chain separated by (a) one epoxide chain and (b) two nearest-neighboring epoxide chains. The supercell of graphene in (a) and (b) contains 48 and 72 carbon atoms, respectively.
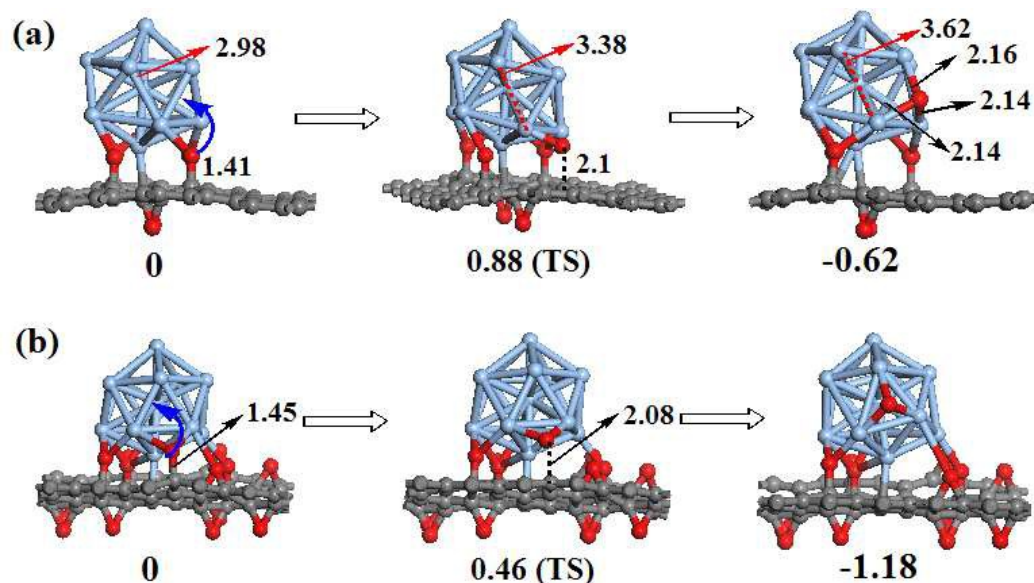
Figure 4 The geometrical structures (distance in Å) of initial state, transition state (TS), and final state for transformation from Ag_{13} to $Ag_{13}O$ on GOs due to the migration of oxygen atom. (a) GO-6O-1 and (b) GO-14-O-1. The blue arrow in initial state defines the migration direction of O. All energies (in eV) are relative to initial state.
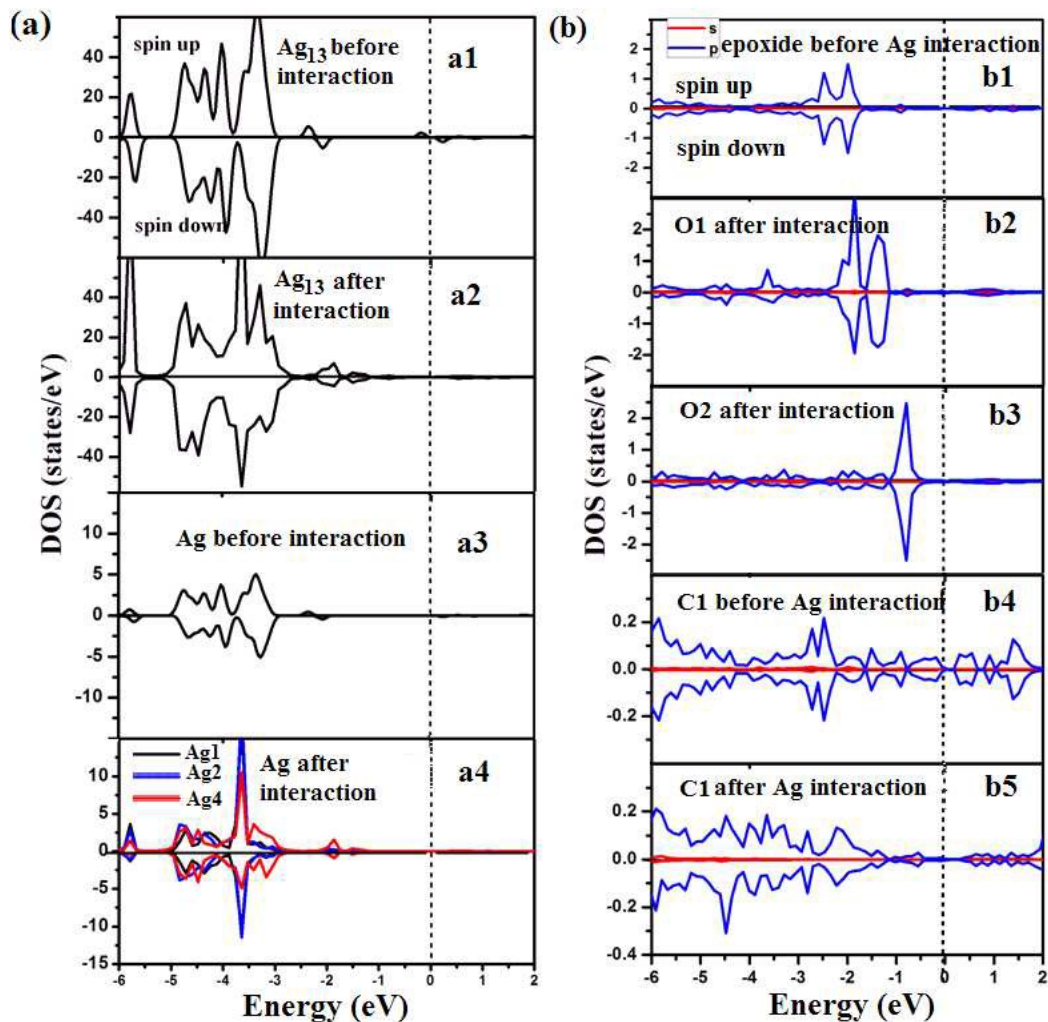
Figure 5 The spin-polarized total DOS (TDOS) and projected DOS (PDOS) for Ag_{13} supported on GO-6O-1. DOS of Ag_{13} before (a1) and after (a2) interaction and PDOS of (a3) Ag from isolated Ag_{13} and (a4) Ag atoms at different sites of adsorbed Ag_{13}. PDOS of (b1) epoxy group and (b4) C1 atom before Ag interaction, (b2) O1, (b3) O2, and (b5) C2 atoms after Ag interaction. The Fermi level is set to 0. The corresponding structure is shown in Figure 1b.
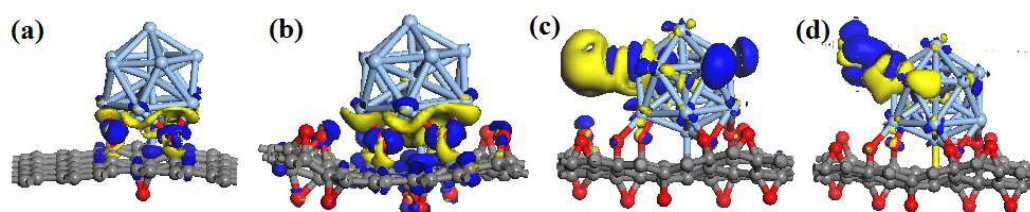
Figure 6 Charge density difference for (a) Ag_{13}/GO-6O-1 and (b) Ag_{13}/GO-14O-1 hybrids and (c) NH_3- and (d) NO-adsorbed Ag_{13}/GO-14O-1 systems. The blue and yellow areas with isosurfaces of 0.003 e/Å^3 present electron accumulation and depletion, respectively.
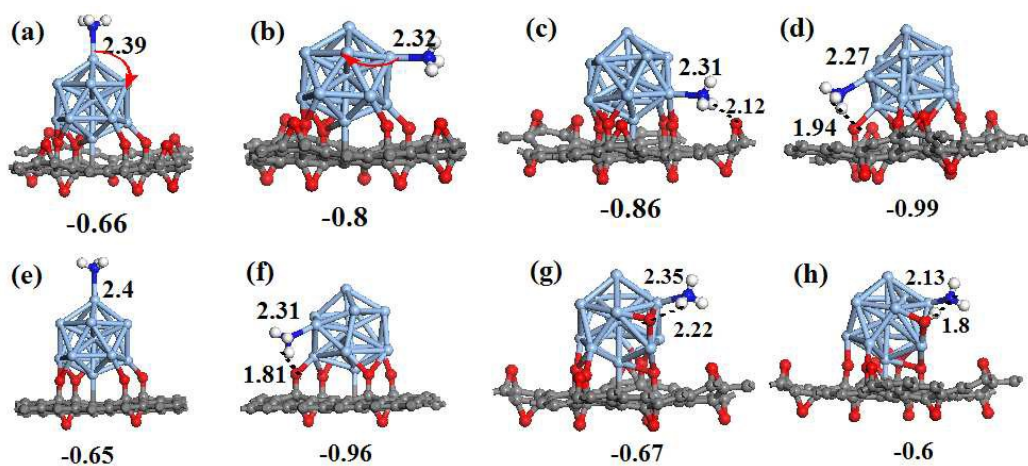
Figure 7 The optimized structures (distance in Å) and corresponding adsorption energies (in eV) for NH_3 adsorbed on (a-d) Ag_{13}/GO-14O-1, (e-f) Ag_{13}/GO-6O-1, and (g-h) $Ag_{13}O$/GO-13O at different sites. (a) and (e) Ag1, (b), (g), and (h) Ag2a, (c) Ag4, and (d) and (f) Ag2b sites. The red arrows in (a) and (b) show the diffusion paths for adsorbed NH_3.
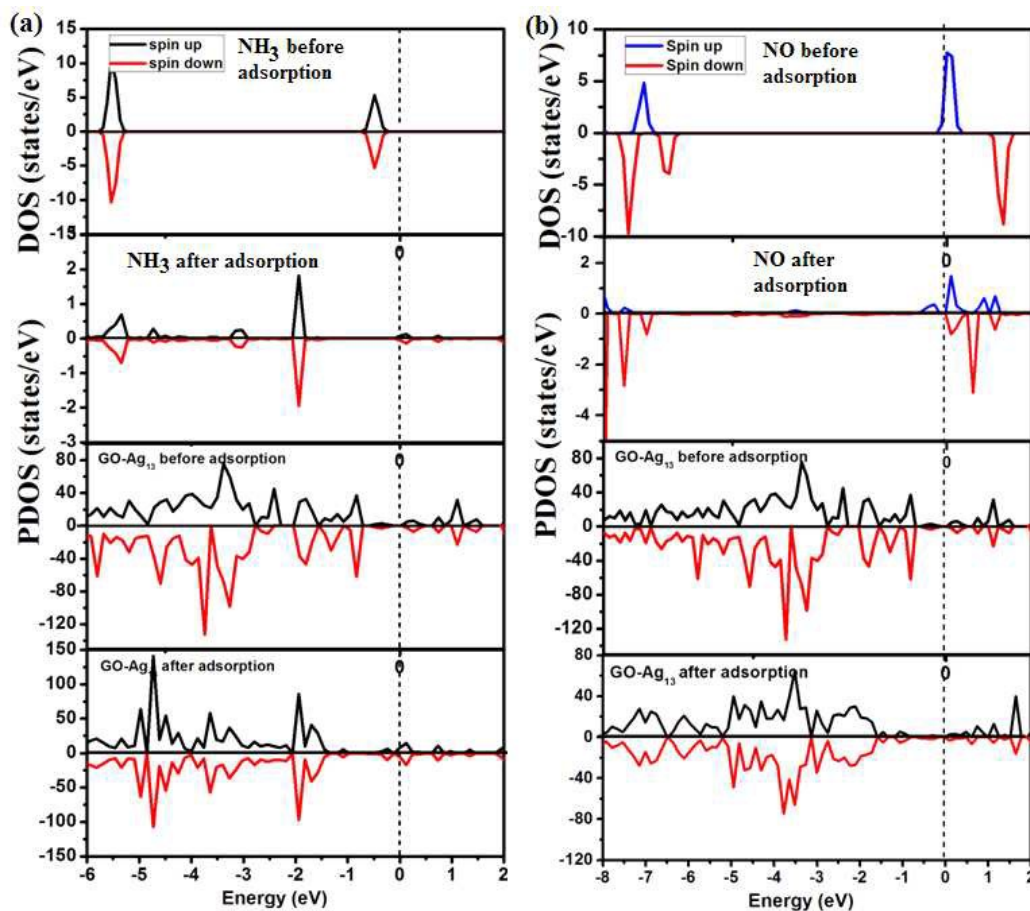
Figure 8 The spin-polarized TDOS and PDOS for (a) NH_3 and (b) NO and Ag_{13}/GO-14O-1 systems before and after gas molecule adsorption. The Fermi level is set to 0.
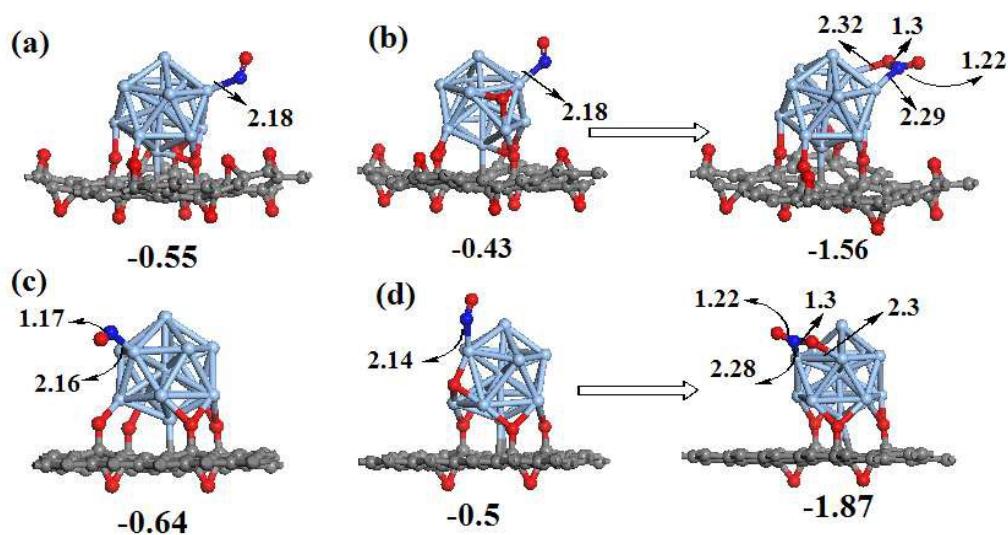
Figure 9 The optimized structures (distance in Å) and corresponding adsorption energies (in eV) for (a) adsorption of NO at Ag2 site and (b) oxidation of adsorbed NO to NO_2 on $Ag_{13}O$/GO-13O. The (c) and (d) for NO adsorption on GO-6O-1 are similar with (a) and (b), respectively.